Methodology for Benchmarking Radio-Frequency Channel Sounders through a System Model*

Camillo Gentile, *Member, IEEE*, Andreas F. Molisch, *Fellow, IEEE*, Jack Chuang, David G. Michelson, *Senior Member, IEEE*, Anuraag Bodi, Anmol Bhardwaj, Ozgur Ozdemir, Wahab Ali Gulzar Khawaja, Ismail Guvenc, Zihang Cheng, François Rottenberg, Thomas Choi, Robert Müller, Niu Han, Diego Dupleich

* Part of this work was presented at the European Conference on Antennas and Propagation 2019.

***Abstract*—Development of a comprehensive channel propagation model for high-fidelity design and deployment of wireless communication networks necessitates an exhaustive measurement campaign in a variety of operating environments and with different configuration settings. As the campaign is time-consuming and expensive, the effort is typically shared by multiple organizations, inevitably with their own channel-sounder architectures and processing methods. Without proper benchmarking, it cannot be discerned whether observed differences in the measurements are actually due to the varying environments or to discrepancies between the channel sounders themselves. The simplest approach for benchmarking is to transport participant channel sounders to a common environment, collect data, and compare results. Because this is rarely feasible, this paper proposes an alternative methodology – which is both practical and reliable – based on a mathematical system model to represent the channel sounder. The model parameters correspond to the hardware features specific to each system, characterized through precision, in situ calibration to ensure accurate representation; to ensure fair comparison, the model is applied to a ground-truth channel response that is identical for all systems. Five worldwide organizations participated in the cross-validation of their systems through the proposed methodology. Channel sounder descriptions, calibration procedures, and processing methods are provided for each organization as well as results and comparisons for 20 ground-truth channel responses.**

***Index terms*— antenna, measurement, propagation, cross-validation, millimeter-wave, mmWave**

I. Introduction

Channel propagation models characterize the physical medium through which radio-frequency (RF) signals travel and so are essential to the design and deployment of wireless communication systems. When developing a wireless standard [1], [2], a preliminary step in the process is to adopt a common channel model so that proposals from participant vendors can be evaluated fairly. As standards evolve with technology, so too must channel models. Notably, interest in directional channels was originally motivated by the development of smart antennas and Multiple-Input Multiple-Output (MIMO) antenna systems in the 1990s. Significant early contributions were made under the COST 259 project [3] and later by 3GPP [4]. Yet, until the late 2000s most efforts focused on bands below 6 GHz [5]. Current interest is strongly linked to recent efforts to develop millimeter-wave (mmWave) wireless technology for Wi-Fi and 5G wireless systems [6]. The World Radio Conference (WRC) 2019 has identified 24.25-27.5 GHz, 37-43.5 GHz, 45.5-47 GHz, 47.2-48.2 and 66-71 GHz as frequency bands for cellular communications in the mm-wave band, though additional frequency bands might be used on a country-by-country basis. A more detailed overview of the history of channel models from 900 MHz to 100 GHz is provided in [7].

Although channel models from legacy standards can sometimes be reapplied, each standard will usually develop its own model because the multiple scenarios, environments, and frequency bands covering the full range of use cases must be captured, requiring data collection for each. For example, while the sub-6-GHz model (with some minor extensions) has been used in 3GPP for the development of the New Radio (NR) Release 15 standard for mmWave bands, a model based more firmly on measurements actually in the mmWave band is desirable. To that end, vendors will often supply measurements from an internal study of use cases most relevant to their products; academic and government laboratories that specialize in channel modeling make contributions to standards as well. Because measurements are time-consuming and expensive to collect, there is considerable interest in comparing and possibly combining contributed data in order to yield more comprehensive results. What is key is that data from various parties is consistent in its format and processing methods. Most importantly, measurements must reflect the channel alone, meaning that the properties of the sounding equipment – e.g. antenna gains and patterns, RF front ends, cables, etc. – must be de-embedded from the measurements, a procedure referred to as *calibration*.

Calibration requires precision instrumentation, especially at the high frequencies in the mmWave regime. Even with

Manuscript received October 11, 2019; revised March 19, 2020; accepted June 03, 2020. Date of publication ###; date of current version ###. Publication of the United States government, not subject to copyright in the U.S. (Corresponding author: Andreas F. Molisch)

C. Gentile, J. Chuang, and A. Bodi are with the Communications Technology Laboratory, National Institute of Standards and Technology, Gaithersburg, MD 20899 USA (e-mail: camillo.gentile@nist.gov, jack.chuang@nist.gov, anuraag.bodi@nist.gov).

A. F. Molisch, Z. Cheng, F. Rottenberg, and T. Choiwas are with the Ming Hsieh Dept. of Electrical Engineering, University of Southern California, Los Angeles, CA, USA. (e-mail: molisch@usc.edu, zihangch@usc.edu, frottenb@usc.edu, choit@usc.edu).

D. G. Michelson and A. Bhardwaj are with the Dept. of Electrical Computer Engineering, University of British Columbia, Vancouver, BC, Canada (e-mail: davem@ece.ubc.ca, anmolb80@ece.ubc.ca).

O. Ozdemir, W. A. G. Khawaja, and I. Guvenc are with the Dept. of Electrical Computer Engineering, North Carolina State University, Raleigh, NC, USA (email: oozdemi@ncsu.edu, wkhawaj@ncsu.edu, iguvenc@ncsu.edu).

R. Müller, N. Han, D. Dupleich are with the Dept. of Electronic Measurements and Signal Processing Group, Technische Universität Ilmenau, Ilmenau, Germany (email: mueller.robert@tu-ilmenau.de, niu.han@tu-ilmenau.de, diego.dupleich@tu-ilmenau.de).

capabilities for precision calibration, no standard procedures exist today and so each organization is bound by its own accord when supplying data, inevitably resulting in non-uniform traits throughout. This presents a significant impediment in the attempt to develop reliable, standardized channel models. Another impediment is the variety of instrument architectures currently used for channel sounding. Although commercial off-the-shelf (COTS) radios are sometimes employed for channel measurements, features of legacy radios – e.g. center frequency, bandwidth, beamwidth – are often not suitable for the design of novel systems. Furthermore, channel data from the radio may not be accessible by or compatible with instrumentation required for calibration. That is why channel sounders typically have a custom, proprietary architecture per organization. This is especially true for mmWave channel sounders for two reasons:

1) the allocated band is very wide (6-100 GHz), lending to numerous combinations of center frequency and bandwidth;
2) mmWave systems will employ directional antennas (because they have high gain) at the transmitter (T) and receiver (R) to recover from the severe pathloss inherent to such high frequencies. In turn, to obtain double-directional channel information – i.e. angle-of-departure (AoD) from the T and angle-of-arrival (AoA) to the R of channel multipath components (MPCs), corresponding to distinct waves propagating between the two – directional antennas are required. Yet directional antennas come in a variety of types: steerable horns, virtual arrays, switched arrays, phased arrays… to name a few.

Aside from instrumentation, the probing signal implemented will affect the measurement outcome, whether it be swept frequency, multi carrier, spread spectrum, chirp, etc. Ultimately, the goal of measurement is to extract the properties of the channel MPCs as primitives for modeling. Super-resolution algorithms – i.e. algorithms that achieve spatial-temporal resolution beyond the Fourier limit inherent to hardware itself, such as CLEAN [8], MUSIC [9], ESPRIT [10], SAGE [11], RiMAX [12], etc., – are widely used in channel sounding for extraction from the measurements and will also affect the results.

How the estimated MPCs will be distorted from the actual channel MPCs will depend on the following list of system features:

- *bandwidth*: the bandwidth of the probing signal – equivalent to its pulse width – will limit the ability to resolve MPCs in delay;
- *signal duration*: the duration of the probing signal – equivalent to the pulse repetition period – will determine the maximum MPC delay that can be measured;
- *dynamic range*: the dynamic range of the probing signal –*i.e.* the difference (in dB) of the 1 dB compression point and the noise floor – will limit the ability to detect weaker MPCs;
- *link budget*: the link budget (transmit power, antenna gain, cable loss, thermal noise, etc.) will limit the ability to detect weaker MPCs from noise and ultimately determine the maximum T-R distance at which the system can operate;
- *beamwidth*: the beamwidth (and pattern) of the antennas will limit the ability to resolve MPCs in angle;
- *field-of-view*: the field-of-view (FoV) of the antenna array – i.e. the range (support) of angles for which, with appropriate steering, an antenna can receive (or transmit) MPCs with a gain no less than a certain threshold below the maximum gain – will limit its ability to "see" MPCs arriving from all angles;
- *polarization*: ideally, sounders should be able to transmit and receive in both vertical and horizontal polarizations or will otherwise not detect cross-polarized MPCs;
- *scan duration*: the time required to steer the antennas to probe all scan directions – the signal duration multiplied by the number of scan directions – sets the maximum mobile speed (and maximum Doppler shift) that can be sustained;
- *sounding duration*: the total time the channel is sounded – the scan duration multiplied by the number of times the scan is repeated – will limit the ability to resolve MPCs in Doppler shift;
- *MPC extraction*: which algorithm is implemented to extract the MPCs will affect their estimated properties;
- *clock drift*: the clock drift will limit the ability to synthesize signals from different antennas when applying super-resolution algorithms;
- *calibration*: the calibration procedures and the precision instrumentation required will affect the reliability of the MPCs estimated.

Hence before combining measurement data or intermediate results obtained with different channel sounders, it is essential to verify that they are comparable. In particular, when individual sounders collect data in different environments, it is important to understand whether the differences in the results observed are due more to the diversity in the channel sounders than to the actual environments themselves. While the simplest approach would be to transport the channel sounders in question to a common environment, collect data, and compare the results, this is rarely feasible.

The 5G Millimeter-Wave Channel Model Alliance [13] – led by the National Institute of Standards and Technology (NIST) – has convened a large number of research labs from around the world to collaborate on standardizing measurement procedures and models for mmWave channels. A subgroup within the Alliance, including researchers from NIST, the University of British Columbia (UBC), the University of Southern California (USC), North Carolina State University (NCSU), and the Technical University of Ilmenau (TUI), has taken up the challenge of devising a practical methodology for benchmarking the quality and resolution of measurements obtained using different channel sounders. The methodology is rooted in a mathematical model to represent the systems. The model parameters are the features listed above, which serve to uniquely characterize the system. A flowchart for the proposed methodology appears in Fig. 1 and can be

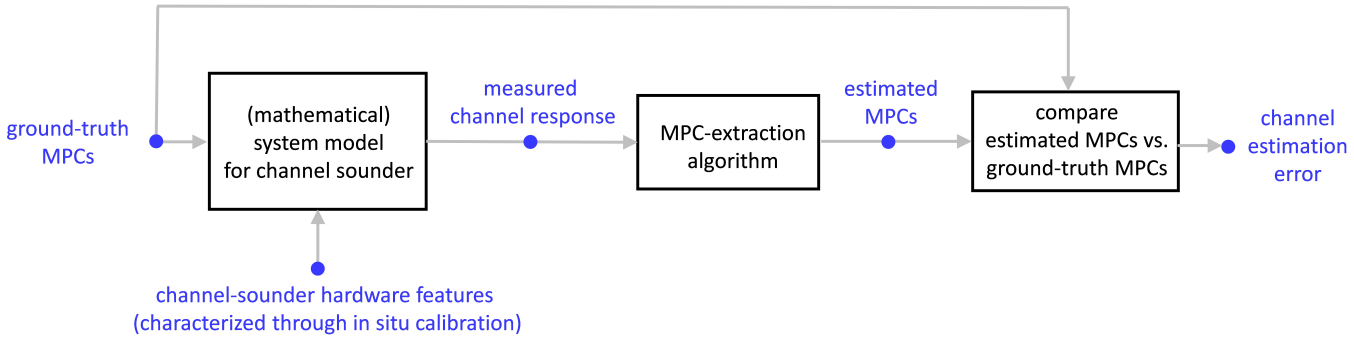

Fig. 1: Flowchart of proposed methodology to benchmark channel sounders.

decomposed into the following four steps:

1) Characterize the hardware features of the channel sounder through precision, in situ calibration. This step is critical for accurate representation by the model;
2) Apply the system model to a ground-truth channel response, expressed as a train of MPCs whose properties are known; this provides a response that is identical for all benchmarked channel sounders to ensure fair comparison. The model output is a response equivalent to what the channel sounder would measure;
3) From the measured response, extract the MPCs and estimate their properties through an appropriate algorithm;
4) Compare the estimated MPCs to the true MPCs.

The effect of the system model will be to "blur" the MPCs, making it difficult to resolve MPCs that are closely spaced in angle, delay, and / or Doppler shift, missing weaker MPCs, and introducing false detections. Discrepancies between the measured MPCs across the sounders will be readily apparent, providing a means to compare their performance against the true MPCs. This approach can potentially provide insights into the sources of error that yield incorrect MPC estimates and possibly suggest strategies for mitigating them.

The remainder of this paper[1] is organized as follows: Section II provides an overview of the channel sounders built by the five participant members and of the calibration procedures employed by each to characterize their hardware. In Section III, the system model as well as how it is applied to the ground-truth channel response are explained. The results of the cross-validation of the channel sounders are presented in Section IV. The last section provides conclusions of the work.

II. DESCRIPTION OF CHANNEL SOUNDERS

The benchmarking methodology proposed in this paper was demonstrated at 28 GHz since the five participant organizations all have mmWave channel sounders at approximately that center frequency. This section provides an overview of the systems, highlighting the variety of approaches and instrument configurations. Details of the calibration procedures to characterize the sounder features are also provided.

[1]A conference version of this work presenting a partial set of results for a limited system model and for the NIST system only is available in [14].

A. National Insitute of Standards and Technology (NIST)

1) System Description: NIST's channel sounder [15] employs a pseudorandom (PN) sequence of length 2^{15} with 1-GHz chip rate (1-ns delay resolution) as the probing signal. The signal is transmitted at 32 dBm Equivalent Isotropically Radiated Power (EIRP) at a center frequency of precisely 28.5 GHz. The T antenna is a 2-dBi dipole with omnidirectional pattern in azimuth (A) and 90º beamwidth in elevation (E); there is no array at the transmitter, thus the system cannot estimate AoD. In contrast, the R has a 16-antenna switched-array system (see Fig. 2(a)): each element is a 16.6-dBi gain horn with 45º beamwidth in the vertical and horizontal planes; the collective FoV over the elements is 360º in azimuth and 90º beamwidth in elevation; because the elements are out-of-plane, both azimuth and elevation AoA can be estimated. All T/R antennas are vertically polarized only. Synchronization in untethered mode is provided through two Rb clocks. The received signal is digitized directly at 40 GHz and matched filtered with the PN sequence to generate a channel impulse response (CIR) per antenna. Matched filtering is performed offline in order to reduce the scan duration to just 66 µs, enabling sounding of mobile channels up to 140 km/h.

The measured CIRs are synthesized coherently through the SAGE algorithm [11], [16] to estimate the path gain, delay, and AoA of the channel MPCs in the following manner: Each MPC appears in the CIRs at slightly different delays due to the different positional offsets of the antenna elements with respect to the array center. AoA is estimated by comparing the delays across the antennas: as the wave approaches, its arrival angle will be closest (farthest) to the boresight angle of the element that detects the path first (last); based on this principle, angles in between are interpolated.

2) System Characterization: Calibration is necessary to de-embed the features of the channel sounder from the measurements (as much as possible) so that the estimated MPCs represent the pure response of the channel alone, not the system. To that end, the system features were first characterized; then calibration of the T/R sections was implemented through pre-distortion filtering: a pre-distorted PN sequence is transmitted in place of the ideal sequence so that what is received after distortion by the system is

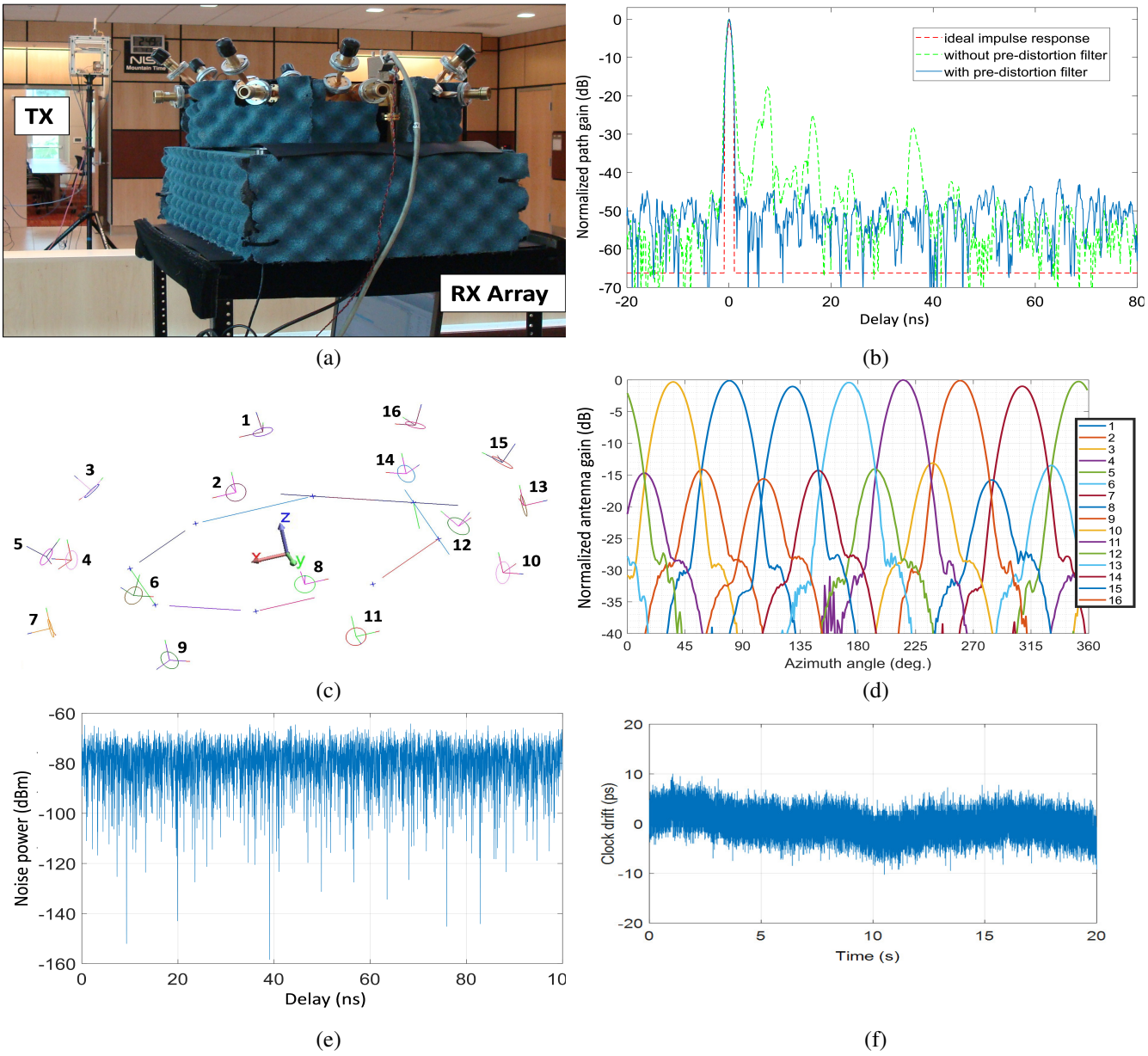

Fig. 2: NIST channel sounder. (a) Photograph. (b) Calibrated channel impulse response, $s(\tau)$. (c) Measured geometry of 16-element receiver antenna array, $x^{(R_j)}$. (d) Measured R azimuth antenna patterns, $g^{R_j,V}(\theta^{R,A})$. (e) Thermal noise, w. (f) Clock drift, w_τ.

ideal[2]. Details of the filter design, including characterization of the transfer functions of the sections through the back-to-back method, are described in [17]. Fig. 2(b) shows the system CIR with and without pre-distortion filtering; the filter removes the spurious peaks and improves the dynamic range of the system to 45 dB, translating to a maximum measurable path loss of 160 dB when considering all factors of the link budget.

The geometry of the R array – i.e. the position and orientation of the 16 antenna phase centers – was measured through a near-field scan using a laser interferometer with 50-nm tolerance [18] (see Fig. 2(c)). The SAGE algorithm relies on known T/R antenna patterns in order to de-embed them from the measurements; accordingly, the patterns were characterized in an anechoic environment with the antennas mounted on the array for enhanced precision; the horizontal cuts for the R antennas are shown in Fig 2(d). The noise floor of the system was characterized by sampling the receiver with the transmitter off; see Fig. 2(e). Finally, the clock drift was gauged by transmitting a continuous-wave signal (narrowband to minimize noise) upconverted to 28 GHz, then downconverted back to IF and digitized while the clocks were free-running (untethered). The drift in the delay of the received sinusoid was sampled in time; see Fig. 2(f); at 28.5 GHz, the 0.38-ps standard deviation in clock drift observed is equivalent to a standard deviation of 3.9° in phase noise.

[2]In reality, the ideal signal can be received only if the system is completely linear, which is never the case for real systems.

B. University of British Columbia (UBC)

1) System Description: UBC's 28-GHz channel sounder has an operating bandwidth of 1 GHz (1-ns delay resolution) [19]. The dynamic range is 45 dB and the maximum measurable path loss is 165 dB. Using a Vector Network Analyzer (VNA), the sounder recorded the frequency response of the channel by transmitting tones across the band of interest (28.5 – 29.5 GHz) and receiving their relative complex amplitude, requiring 500 ms to probe the whole band. A photograph of the system during field measurements and a block diagram of the system components are shown in Fig. 3. The Block Up Converter (BUC) was used to up-convert the 1 GHz IF signal from the VNA to 30 GHz. On the receiver side, the 30 GHz signal was down-converted to 1.25 GHz using a mixer. A Voltage Signal Generator (VSG), comprised of a frequency doubler, was used as a local oscillator. To maintain synchronization between the BUC and the receiver, the 10 MHz reference signal generated by the VNA was injected to the fiber link (using bias T) and delivered to the transmit side. After amplification, the 10 MHz signal was then injected back to the BUC, along with 24 V DC power, using bias T.

The T antenna is a dual-polarized 18-dBi horn with 20º beamwidth in both planes; the R antenna is a dual-polarized 23-dBi horn with 13º beamwidth in both planes. Both antennas are mounted on rotators[3] for double-directional scanning in azimuth with 360º scan range. A double-directional scan is conducted in the following manner: In a first pass, all AoD/AoA pairs are scanned using a single tone only (at the center frequency) to decrease the scan duration. The next step is to identify the five pairs with the highest signal strength; the underlying assumption is that most of the received power will be concentrated in just a few directions. In a second pass, the positioners return to the five dominant AoD/AoA pairs identified and the frequency response across the whole band is recorded for each; from the frequency response, the CIR is computed through the Inverse Fourier Transform. The peaks in the CIRs are identified as unique channel MPCs; accordingly, all peaks will have the same double-directional angle estimated as the AoD/AoA of the pair. The total scan duration, comprising first and second passes, requires 20 minutes.

2) System Characterization: Calibration of the channel sounder was realized through the back-to-back method in which the antennas were disconnected from the system and T and R front ends were connected directly at the antenna connection planes through an attenuator; the frequency response, $H^{B2B}(f)$, was then recorded. In a separate step, the frequency response of the attenuator was characterized as $H^{ATT}(f)$. A calibrated frequency response was subsequently obtained by dividing the frequency response measured with the antennas by $H^{B2B}(f)/H^{ATT}(f)$.

The principal plane patterns of the T/R antennas were furnished by the manufacturer and were interpolated in between to provide 3D patterns in azimuth and elevation. The patterns were necessary to de-embed the antenna gains at the scanned AoD/AoA angles from the calibrated frequency response.

[3]J-Systems® JPTH-13M model with 0.15° tolerance.

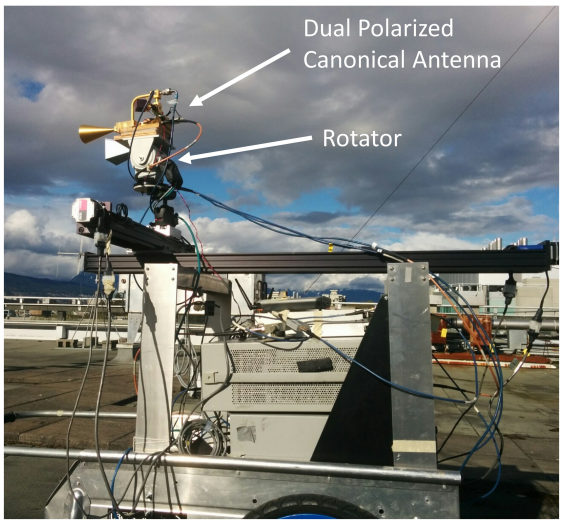

(a)

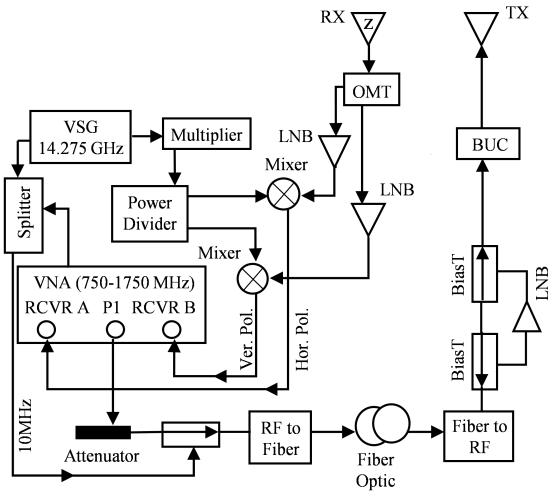

(b)

Fig. 3: UBC channel sounder. (a) Photograph. (b) Block diagram.

C. University of Southern California (USC)

1) System Description: Block diagrams of USC's phased-array based 28-GHz channel sounder (jointly developed with Samsung) [20] are shown in Fig. 4. It has an operating bandwidth of 400 MHz (2.5 ns delay resolution). The multi-carrier probing signal with modified Newman phases (to minimize the Peak-to-Average Power Ratio (PAPR)) is generated from an internal FPGA, yielding a dynamic range of 77 dB. The sounder can realize an electronic double-directional scan (19 x 19 T/R beam pairs) within 1.44 ms due to its fast beam-switching capabilities (< 2 μs). Separate free-running GPS reference clocks on the T and R were used for synchronization.

With a maximum EIRP of 57.1 dBm and R beam gain of 19.5 dBi, the maximum measurable path loss is 160 dB. The T/R antennas are both 8 × 2 phased arrays capable of resolving AoD/AoA, respectively. While both azimuth and

elevation can in principle be resolved, currently calibration is only available for azimuth. The array presents 12º beamwidth in azimuth and 22º beamwidth in elevation over a beam range of +/-45º in azimuth in 5º beam steps. The beam switching pattern, averaging, etc., are all configurable within the FPGA. The FoV of each array board is just 90°; if this is sufficient for the measurement at hand, the scan duration is as low as 15 ms. If extension of the FoV to 360° is desired, the board is rotated to four different orientations (per end), increasing the scan duration to minutes.

2) System Characterization: Super-resolution estimation of MPC properties requires knowledge of the antenna patterns. In most sounders, an antenna can be characterized by disconnecting it from the sounder, connecting it to the T port of a VNA, and measuring the signal received by a reference antenna connected to the R port. In this case, both excitation and reception are at the nominal operation frequency of the sounder, e.g. 28 GHz. However, for the USC sounder the phased arrays are integrated with RF electronics – such as amplifiers, embedded mixers, and local oscillators at 26 GHz – on a printed circuit board (PCB) in a box, which we call the RFU. A further difficulty arises from the fact that the system characteristics might depend on the gain settings of the amplifiers. Therefore, a new calibration method based on over-the-air (OTA) techniques is proposed in [21].

The multi-gain calibration we implemented is summarized here as follows: A horn antenna operating at 28 GHz is used as a reference while measuring the beam patterns of the T and R RFUs separately. As the sweeping frequencies at the horn antenna and RFUs are different (the RFUs only accept intermediate frequency as an input, which is in the 2-3 GHz range), frequency conversion was necessary. Each RFU beam pattern was traced out by mechanically rotating the array in azimuth on a turntable, at different gains. After compensating for the boresight gain of the beams and the free-space path loss, the frequency response at each gain setting was recorded. All the while, a Rb reference of 10 MHz was shared between the horn, the RFUs, and the VNA.

From the calibration data, the Effective Aperture Distribution Function (EADF) was computed to characterize the array for the RiMAX algorithm [12]. The output of the algorithm is a set of estimated MPCs and associated properties that best reconstruct – in the maximum likelihood sense – the observed frequency responses at all double-directional scan angles. The phase drift of the clocks was characterized with a standard deviation of just 4º over the 1.44-ms scan; this is critical for super-resolution parameter estimation when the T and R are untethered.

D. North Carolina State University (NCSU)

1) System Description: NCSU's channel sounder is based on National Instruments' (NI) 28-GHz equipment; see Fig. 5(a). It consists of T/R chassis and radio heads as well as Rb clocks and rotatable antenna gimbals. The probing signal is a Zadoff-Chu (ZC) sequence of length 2048, oversampled by a factor of 2 followed by a root raised cosine (RRC) filter before conversion to analog at sample rate f_s = 3.072

(a)

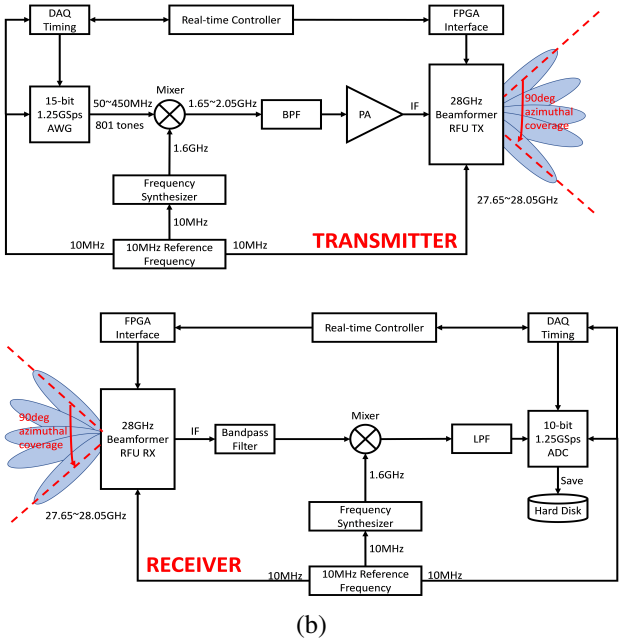

(b)

Fig. 4: USC channel sounder. (a) Photograph of RFU. (b) Block diagram.

GS/s; delay resolution is $2/f_s$ = 0.65 ns with signal duration of 2048 x 0.65 ns = 1.33 µs. In tethered mode, a 10 MHz pulse per second (PPS) signal from a single Rb clock is shared by the T and R to generate the local oscillator (LO) signals and to simultaneously trigger transmission and reception. Untethered mode requires an initial training between the two Rb clocks for synchronization. Baseband-to-RF up-conversion and RF-to-baseband down-conversion are performed in separate stages. The analog-to-digital converter has 60-dB dynamic range. The T/R antennas are both 17 dBi horns with 24º beamwidth in azimuth and 26º beamwidth in elevation. Altogether, path loss up to 185 dB can be measured.

The T and R antenna gimbals are mounted on identical azimuth-elevation positioners for double-directional scanning: the azimuth plane is scanned 360° in 20° steps while the elevation plane is scanned at -20°, 0°, and 20°, resulting in a total number of $(18x3)^2$ = 2916 AoD/AoA pairs. Channel MPCs are extracted from the scans in the following manner: First, all peaks in the scanned CIRs 20 dB above the noise floor are identified. The peaks arriving at the same

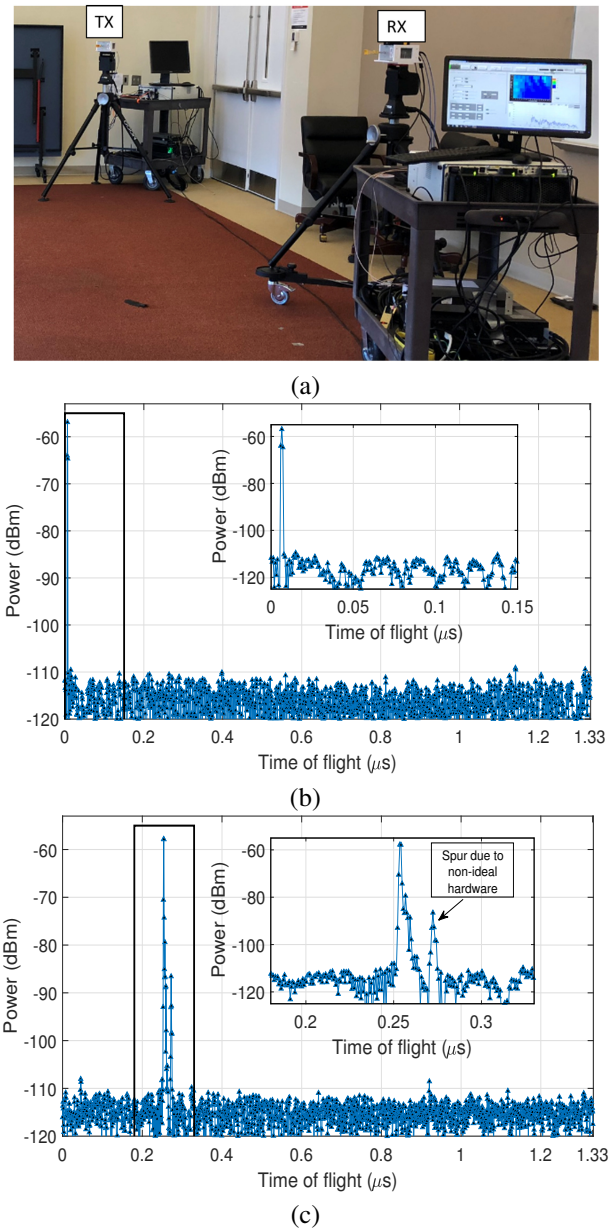

Fig. 5: (a) NCSU channel sounder. (b) CIR obtained due to non-ideal hardware. (c) CIR after calibration.

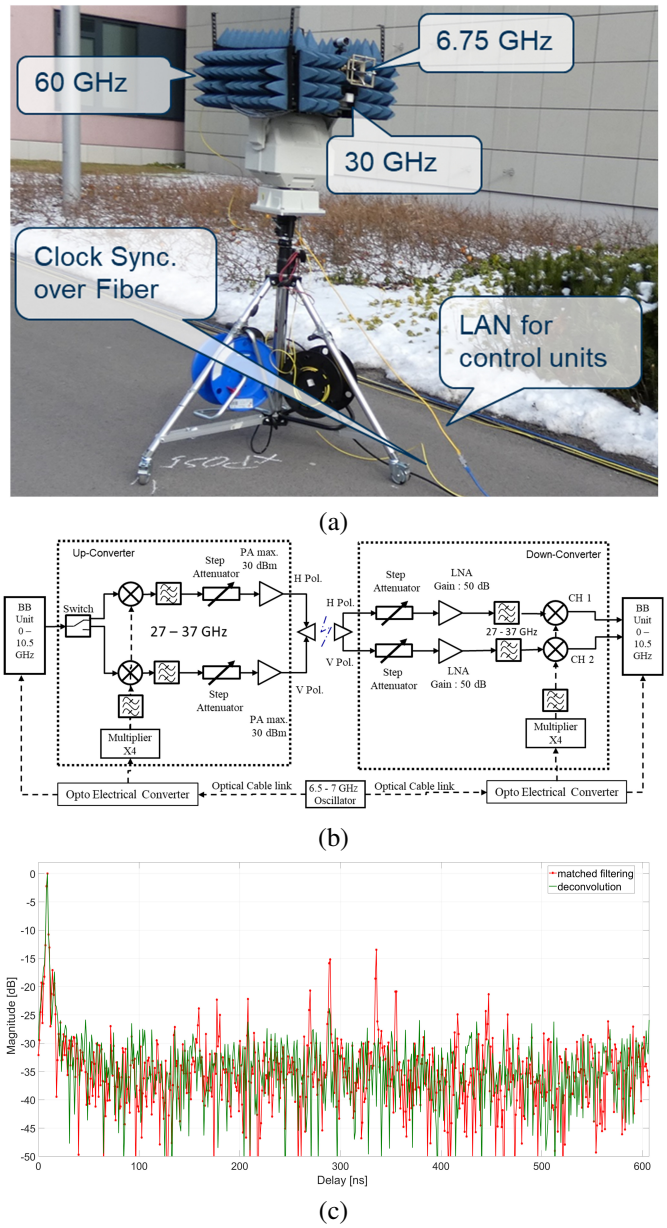

Fig. 6: TUI channel sounder. (a) Photograph. (b) Block diagram. (c) Calibration of impulse response.

delay across the scans are dismissed as originating from the same MPC, whose AoD/AoA is given by the scan angles with the highest peak power; thus the estimated AoD/AoA are constrained to the double-directional scan angles. This procedure is repeated for all delays where peaks are detected.

2) System Characterization: The non-ideal hardware introduced spurs into the CIRs, as illustrated in Fig. 5(b). Consequently, the hardware response had to be characterized and calibrated. The details of the back-to-back method to do so are provided in [22], [23]. In brief, a cable with a 40-dB attenuator (to protect the receiver from saturation damage) was connected between the T and R radio heads. The measured response was then deconvolved from the ideal response. After calibration, no spurs were observed in Fig. 5(c).

The T/R antennas patterns used to adjust the power of the extracted MPCs to the free-space baseline were furnished by the manufacturer specifications.

E. Technical University of Ilmenau (TUI)

1) System Description: Technical University of Ilmenau's channel sounder is composed from a number of subsystems, ranging from microwave up to the lower Terahertz bands. The subsystems allow for simultaneous measurement of three different frequency bands – 3-10 GHz, 30-37 GHz, and 57-64 GHz bands – at the same location with an instantaneous 10-dB bandwidth of 6.75 GHz (0.14-ns delay resolution). The probing signal is a maximal length PN sequence of 212 bits, translating to an alias-free delay range of 600 ns. An optical system was employed for distributing a 7-GHz clock,

TABLE I: MAIN FEATURES OF FIVE PARTICIPANT CHANNEL SOUNDERS

	Center freq. (GHz)	Band–width (GHz)	Probing signal	Dynamic range (dB)	T power (dBm)	Antenna gain (dBi)	Antenna beamwidth (deg.)	Pol.	Max meas. path loss (dB)	Directional Scan	Scan duration	FoV (deg.)
NIST	28.5	1	2^{15} M–ary sequence	45	30	2 (T) 16.6 (R)	360 (T,A) 90 (T,E) 45 (R,A) 45 (R,E)	V (T,R)	160	(R,A/E) electronic	66 μs	360 (T,A) 90 (T,E) 360 (R,A) 90 (R,E)
UBC	28	1	VNA–based frequency sweep	45	46	18 (T) 23 (R)	20 (T,A) 20 (T,E) 13 (R,A) 13 (R,E)	V (T,R) H (T,R)	165	(T/R,A) mechanical	20 min	360 (T,A) 95 (T,E) 360 (R,A) 88 (R,E)
USC	27.9	0.4	FPGA–based frequency sweep	77	37.6	19.5 (T) 19.5 (R)	12 (T,A) 22 (T,E) 12 (R,A) 22 (R,E)	V (T,R)	160	(T/R,A) electronic/ mechanical	minutes	360 (T,A) 22 (T,E) 360 (R,A) 22 (R,E)
NCSU	28	1.5	2^{11} Zadoff–Chu sequence	60	10	17 (T) 17 (R)	24 (T,A) 26 (T,E) 24 (R,A) 26 (R,E)	V (T,R)	185	(T/R,A/E) mechanical	30 min	360 (T,A) 66 (T,E) 360 (R,A) 66 (R,E)
TUI	30	7	2^{12} M–ary sequence	60	30	21 (T) 21 (R)	15 (T,A) 15 (T,E) 15 (R,A) 15 (R,E)	V (T,R)	220	(R,A/E) mechanical	hours	15 (T,A) 15 (T,E) 360 (R,A) 165 (R,E)

providing synchronization to the baseband units and the RF converter of the T and R stations up to several hundreds of meters. Fig. 6(a) displays a photograph of the fully integrated system [24].

A schematic of the 30-GHz subsystem is illustrated in Fig. 6(b). The structure of the channel sounder is based on a superheterodyne principle, featuring automatic gain control (AGC) at the R to extend dynamic range beyond 60 dB. The maximum T output power is 30 dBm and the T/R antennas have 21-dBi gain (15° half-power beamwidth), translating to a measurable path loss of 220 dB. The R antenna is mounted on azimuth-elevation positioners for AoA scanning at 0.1º steps: -180º to +180º in azimuth and -75º to +75° in elevation. The system features dual polarization in parallel at the R and switched dual polarization at the T side. The full system has one T station and two R stations such that two locations can be measured in parallel. The scan duration is several hours, hence only static environments can be sounded.

The MPCs are extracted by identifying peaks in the scanned CIRs. A real MPC will not only generate a peak in a single scan angle, but also in adjacent scan angles at the same delay: the closer the scan angle to the direction of the MPC, the stronger the peak power. This relationship is used to map out the power detected across multiple scan angles at the same delay and to interpolate in between, providing an angular resolution of 1°.

2) System Characterization: The probing signal was calibrated in two phases: Phase 1 consisted of a back-to-back measurement using 160-dB coaxial attenuators, characterized through precision VNA measurements. Calibration was subsequently implemented through deconvolution of the back-to-back reference from the matched-filter response. Phase 2 consisted of in situ measurements for time alignment (based on the known T-R distance) and for power calibration (based on the known path loss from Friis transmission equation, which is a function of that distance). Fig. 6(c) displays the calibrated CIR in line-of-sight (LOS) conditions; spurious peaks, noticeable before calibration, vanish after deconvolution is applied.

In addition to calibration of the CIR, the T and R antenna patterns were characterized in an anechoic chamber. Finally, the coherent, low-jitter clock was gauged to have single-side band phase noise of -100 dBc/Hz at 1 kHz from the carrier.

The salient features of the five participant channel sounders are summarized in Table I.

III. SYSTEM MODEL

The features characterized in the previous section were used as parameters of the system model to represent the channel sounders. This section describes the model and how it was applied to the ground-truth channel response.

A. Ground-Truth Channel Response

Numerous industrial consortia [2], [13], [25]–[27] have subscribed to map-based channel models [28] for mmWave systems, such as the Quasi-Deterministic (QD) model [38]. This is because at such high frequencies diffraction can be neglected [30], [31], leaving direct transmission and specular reflection, whose geometrical properties can be computed efficiently through raytracing given a map of the environment – hence the model name. In our study, the ground-truth channel response was generated from the QD model of a

19 m × 10 m × 3 m lecture room in LOS conditions, assuming omni-directional FoV in azimuth and elevation at both the T and R. The response was expressed as a train of polarization-dependent raytraced MPCs – with zero noise, unlimited spatial-temporal resolution, and 100-dB dynamic range – under the narrowband assumption (for which the frequency response of each MPC is flat across the band). The path gain for the direct path was given from free-space propagation (characterized through Friis transmission equation) plus reflection loss for specular paths from the ceiling, ground, and walls (characterized through measurement [32]). Reflections above second order were discarded since their path loss exceeded that of the direct path by more than 40 dB, contributing little to the total channel power while increasing complexity significantly. In all, there was a total of 21 specular reflections. Fig. 7(a) shows raytraced MPCs for a test T-R location.

The QD model also accounts for diffuse reflections due to surface roughness: a cluster of diffuse MPCs associated with each specular path was generated stochastically, multiplying the total number of ground-truth paths from 21 to nearly 400 altogether. The stochastic properties of the clusters, such as angular spread ($\sim$ 3º) and the relative strength of the diffuse reflections with respect to the specular reflections ($\sim$ 6 dB), were also characterized through measurement. Since the diffuse paths were packed densely in the delay-angle space, they were pivotal in benchmarking the resolution of the systems.

For the n^{th} path in the response, the following properties were rendered by the model:

- polarization-dependent complex amplitude a_n^{pq}, where p denotes either the vertical (V) or horizontal (H) polarization of the T antenna and q denotes that of the R antenna;
- delay τ_n;
- AoD $\boldsymbol{\theta}_n^T = [\theta_n^{T,A}\ \theta_n^{T,E}]$ and AoA $\boldsymbol{\theta}_n^R = [\theta_n^{R,A}\ \theta_n^{R,E}]$ in azimuth and elevation.

Fig. 7(b) shows a projection of the paths (direct, specular, and diffuse) into the delay-angle property space of the MPCs.

It is worth noting that the ground-truth channel model presented here is for the purpose of illustrating the proposed methodology and, in general, other channel models can be employed – with MPCs restricted to within a given FoV, polarization, dynamic range, etc. – if they are geared towards a particular application.

B. Description of System Model

Consider a T antenna array centered at $\boldsymbol{x}^{T_0}$ and a R array centered at $\boldsymbol{x}^{R_0}$. A generic model for the arrays is shown in Fig. 8, where $\boldsymbol{x}^{T_i}$ and $\boldsymbol{x}^{R_j}$ are the respective positions of the i^{th} transmit and j^{th} receive elements [4]. It follows that the relative delay of the n^{th} path at $\boldsymbol{x}^{T_i}$ with respect to $\boldsymbol{x}^{T_0}$ is given by

$$\tau_n^{T_i} = \frac{u(\boldsymbol{\theta}_n^T) \cdot (\boldsymbol{x}^{T_0} - \boldsymbol{x}^{T_i})}{c} \tag{1}$$

[4]For example, see characterization for NIST system in Fig. 2(c).

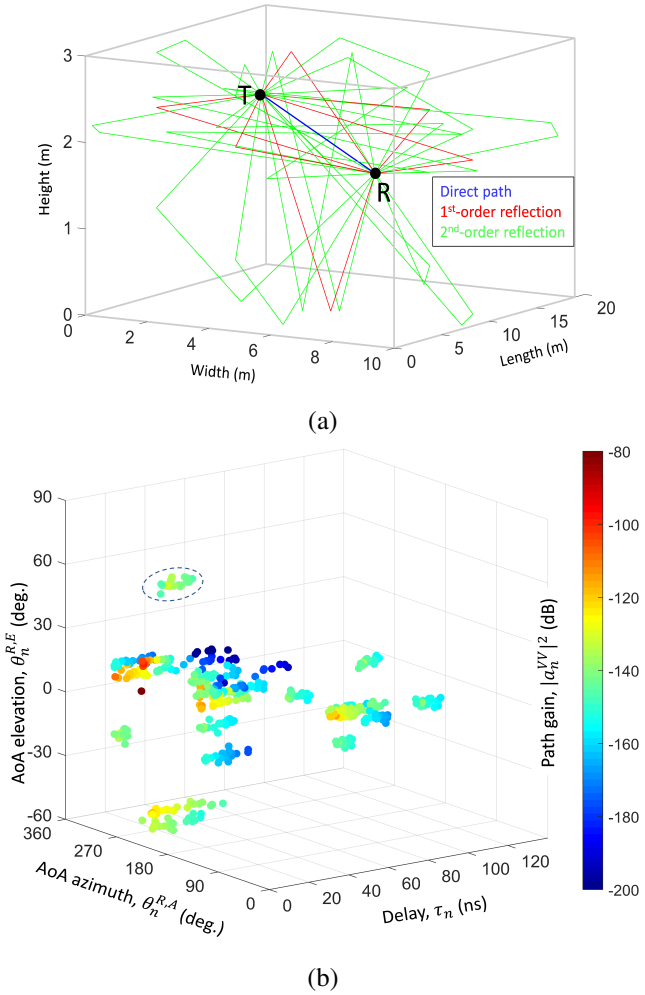

(a)

(b)

Fig. 7: Quasi-Deterministic channel model. (a) Visualization of raytraced paths in the 19 m x 10 m x 13 m lecture room; besides the direct path, there are six 1st -order reflections and 15 2nd -order reflections. (b) Paths projected into the delay-angle space; each specular path has an associated cluster of MPCs originated from diffuse scattering; the cluster from the 1st -order ceiling reflection is highlighted.

and its relative delay at $\boldsymbol{x}^{R_i}$ with respect to $\boldsymbol{x}^{R_0}$ is given by

$$\tau_n^{R_j} = \frac{u(\boldsymbol{\theta}_n^R) \cdot (\boldsymbol{x}^{R_0} - \boldsymbol{x}^{R_j})}{c}, \tag{2}$$

where

$$u(\boldsymbol{\theta}) = \begin{bmatrix} \cos(\theta^A) \cdot \sin(\theta^E) \\ \sin(\theta^A) \cdot \sin(\theta^E) \\ \cos(\theta^E) \end{bmatrix} \tag{3}$$

is the unit angle vector. The complex amplitudes of the antenna patterns[5] are defined as $g^{T_i,p}(\boldsymbol{\theta}^T)$ and $g^{R_j,q}(\boldsymbol{\theta}^R)$. The generic model accounts for displacement of antenna elements in real arrays [15], [16], [33], [44] (NIST) or virtual arrays [35], [36]. The model also accounts for antenna steering through electrical scanning [20], [21], [36] (USC) or mechanical scanning [19], [22]–[24], [38]–[43] (UBC, NCSU, TUI).

Now let $s(\tau)$ be the calibrated channel impulse response[6]

[5]For example, see characterization for NIST system in Fig. 2(d).

[6]For example, see characterization for NIST system in Fig. 2(b).

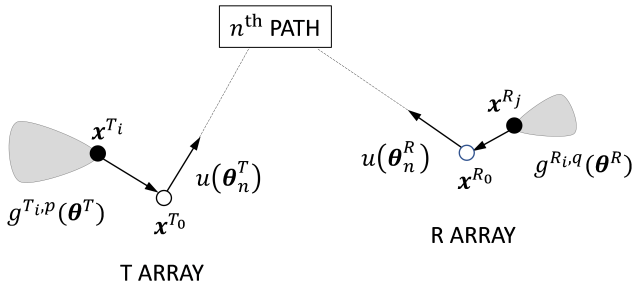

Fig. 8: Generic antenna geometry and antenna patterns for the T and R antenna arrays of the system model.

(NIST, NCSU, TUI) – or the equivalent delay-domain representation of the calibrated frequency response (UBC, USC) – and let f_c be the center frequency for the narrowband system. Then the polarization-dependent received signal at R_j from T_i is

$$y_{ij}^{pq}(\tau, \boldsymbol{\theta}^T, \boldsymbol{\theta}^R) = \sum_{n=1}^{N} s(\tau - \tau_n - \tau_n^{T_i} - \tau_n^{R_j} + w_\tau) \cdot e^{j2\pi f_c(-\tau_n - \tau_n^{T_i} - \tau_n^{R_j} + w_\tau)} \cdot a_n^{pq} \cdot g^{T_i,p}(\boldsymbol{\theta}^T - \boldsymbol{\theta}_n^T) \cdot g^{R_j,q}(\boldsymbol{\theta}^R - \boldsymbol{\theta}_n^R) + w. \quad (4)$$

For the n^{th} path of the ground-truth channel response, the probing signal is shifted by a composite delay due to propagation between the array centers (τ_n) plus the relative delays from the array centers to the antenna elements $(\tau_n^{T_i}, \tau_n^{R_j})$; the composite delay imparts a phase shift on the signal as well. The signal is then modulated by the complex amplitude of the channel and by the T/R antennas gains and then summed over all paths. Random variables for thermal noise[7], w, and clock drift[8], w_τ, modeled as Gaussian processes were added.

C. Application of System Model

As an example, consider application of the NIST system model to a ground-truth channel impulse response. Fig. 9 shows the signal $y_{1j}^{VV}(\tau, \boldsymbol{\theta}_1^T, \boldsymbol{\theta}_j^R)$ received at three adjacent antennas ($j = 6, 7, 8$) of the 16-element R array. The direct path (n = 1) is detected first (at 13.38 ns) by element 7 since its arrival angle is closest to the boresight angle of that element and is proportionally detected next by element 6 (at 13.40 ns) and then by element 8 (at 13.53 ns). Given the directional antennas, the signal strengths for $j = 6, 7, 8$ are (-29.14, -30.89, -37.74) dBm. The received signals are processed by the SAGE algorithm to yield the estimated properties $(\hat{a}_n^{VV}, \hat{\tau}_n, \hat{\boldsymbol{\theta}}_n^R)$, visualized in Fig. 11(a).

The other sounders in this study have single antennas at the T and at the R: the directional patterns of USC's phased arrays are steered electronically towards distinct double-directional scan angles whereas the fixed horns of the other three systems (UBC, NCSU, TUI) are steered mechanically. Each double-directional scan $(\boldsymbol{\theta}_k^T, \boldsymbol{\theta}_l^R)$ yields a distinct received signal $y_{11}^{pq}(\tau, \boldsymbol{\theta}_k^T, \boldsymbol{\theta}_l^R)$, which are collectively processed via the algorithms described in Section II to estimate the properties of the extracted MPCs. Even with a single antenna, care shall be taken for accurate system representation: For example, the axis of rotation of NCSU's horns is 20 cm, which is significant with respect to the system's 1-ns delay resolution (corresponding to 30 cm). This means that antennas will effectively have different positions per scan (like the NIST system) and so the same MPC will arrive with different delays in the measured responses.

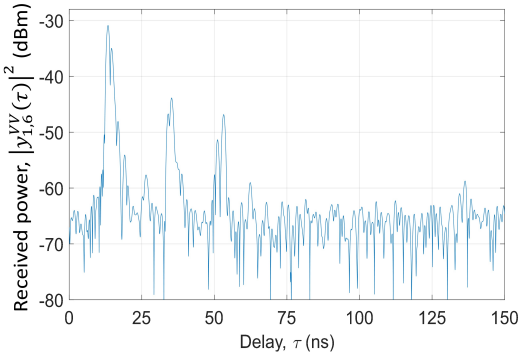

(a)

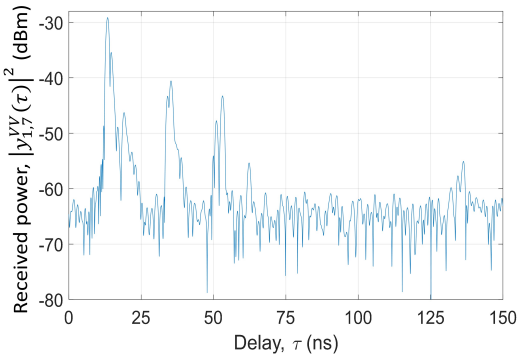

(b)

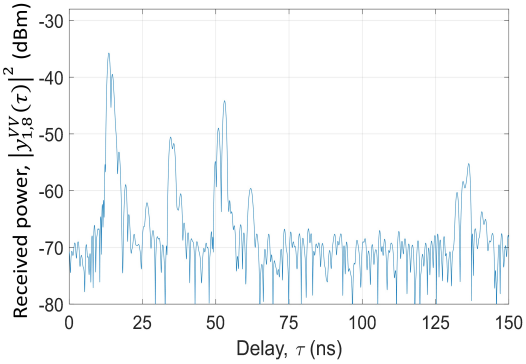

(c)

Fig. 9: Received signal $y_{1j}^{VV}(\tau, \theta_i^T, \theta_j^R)$ at three adjacent R elements $j = 6, 7, 8$ generated from a ground-truth channel response applied to the system model for NIST's channel sounder.

[7]For example, see characterization for NIST system in Fig. 2(e).
[8]For example, see characterization for NIST system in Fig. 2(f).

D. Extensions of System Model

As mentioned early, an important feature of channel sounders is scan duration, which for some systems is on the order of minutes or even hours due to mechanical rotation or translation to capture directional channels, limiting their application to static environments only. In this study, the channel was assumed to be static, but could be readily extended to dynamic channels by making the T and/or R mobile, resulting in time-varying ground-truth MPCs. The channel would then be sampled over time – as the sounder would – by implementing multiple scans in the sounding duration for the purpose of evaluating how well the system estimates time-varying channels, in particular Doppler shift of the MPCs.

As a rule of thumb, the narrowband assumption holds when the signal bandwidth is less than 10% of the center frequency. This is obviously not valid for TUI's system. In fact, TUI demonstrated frequency selectivity across the 7-GHz band for scatterers such as metal [44]. Frequency selectivity across a 14-GHz band was also demonstrated in [36]. As of now, the nature of this selectivity at such large mmWave bandwidths is not well understood due to lack of extensive measurements, but in the future can be incorporated as an additional MPC property [45]. Also, mmWave systems will employ massive-MIMO phased-array antenna in order to generate pencilbeams with very high gain [46]; the length of the aperture may be tens or hundreds of wavelengths, for which the plane-wave assumption is no longer valid; accordingly, the MPCs can be modeled as spherical waves, albeit demanding more advanced approaches than raytracing to generate the ground-truth channel response.

For systems with free-running clocks that have sounding durations on the order of minutes or more, the long-term component of the clock drift (in minutes or hours as opposed to milliseconds or seconds) must also be taken into account in w_τ in (4); for example, the component is deterministically linear for Rb. Random variables for uncertainty in position of the antenna elements and in the complex amplitude of the antenna patterns can also be factored into (4), however with precision instrumentation and calibration procedures, their effect would be dwarfed by other random components (thermal noise and clock drift) and thus have been omitted in this study. Finally, since the instruments operate in the linear regions of their components, non-linear distortions have been neglected but can indeed be accounted for, albeit complicating the current linear model significantly.

IV. RESULTS

The results of the cross-validation between the five participant channel sounders are presented in this section. For this effort, ground-truth channel responses were generated for 20 test scenarios: ten with different T-R locations in the lecture room with fixed T and R antenna heights of 2.5 m and 1.6 m, respectively; an additional ten scenarios were generated in the same room, however by doubling the room dimensions. Then the MPCs estimated by each system were compared against the ground-truth MPCs through two means: first, common large-scale channel metrics were calculated across all paths; then the paths were compared one by one in terms of their properties.

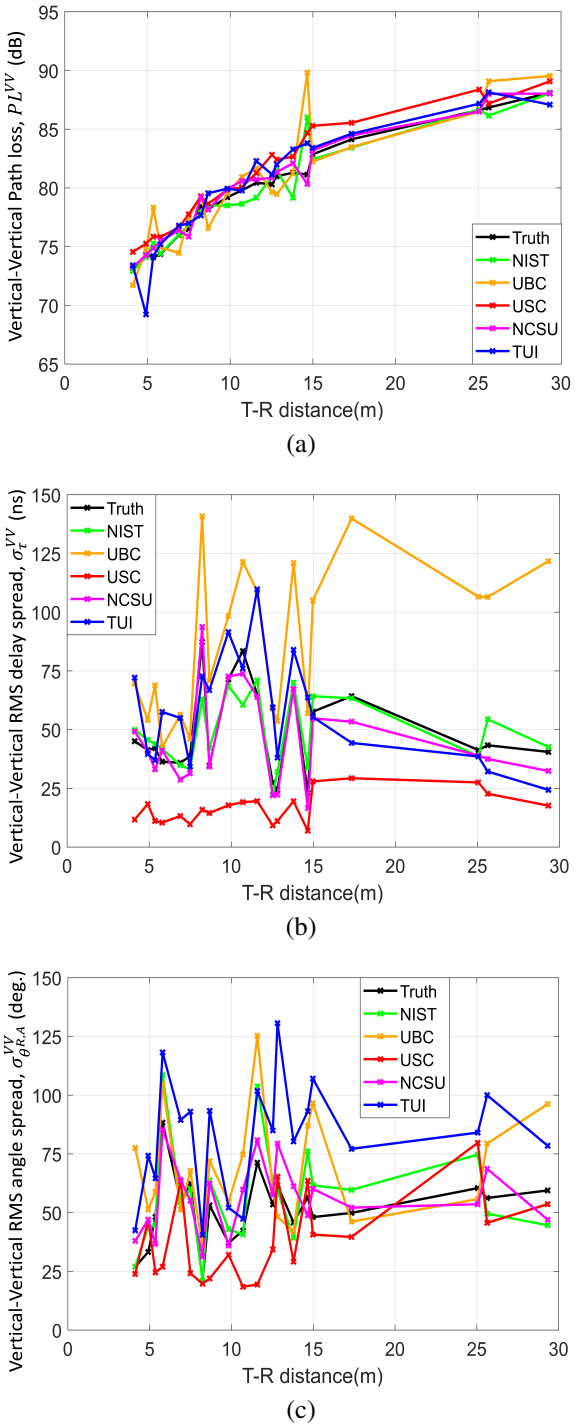

Fig. 10: Comparison of large-scale statitics estimated from five channel sounders to ground-truth statistics. (a) Vertical-Vertical Path loss (b) Vertical-Vertical RMS delay spread (c) Vertical-Vertical RMS angle spread.

A. Large-Scale Channel Metrics

The cross-validation could be conducted based only on the MPC properties common to all five systems, which in this case were complex amplitude of the vertical-vertical

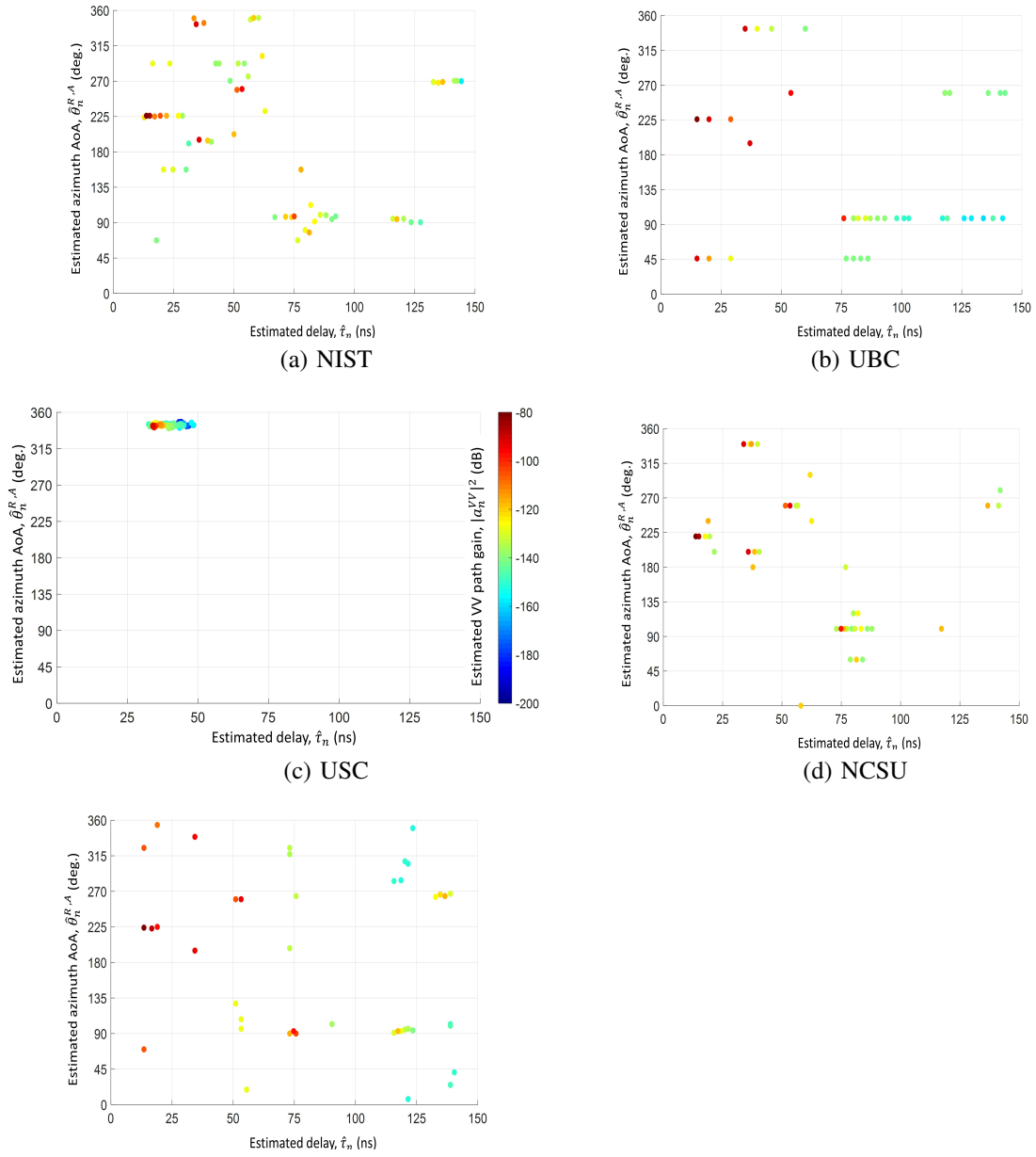

(a) NIST (b) UBC

(c) USC (d) NCSU

(e) TUI

Fig. 11: MPCs estimated (shown as outlined, shaded circles) by the channel sounders of the five participant organizations. Results are only shown in the MPC property space shared by all systems $(a_n^{VV}, \tau_n, \theta^{R,A})$ for the test scenario corresponding to the true MPCs (also shown, as not-outlined, semi-transparent shaded circles) in Fig. 7(b).

polarization (a_n^{VV}), delay (τ_n), and azimuth AoA ($\theta^{R,A}$). Fig. 10(a-c) displays the vertical-vertical pathloss (PL^{VV}), the vertical-vertical RMS delay spread (σ_τ^{VV}), and the vertical-vertical RMS angle spread ($\sigma_{\theta^{R,A}}^{VV}$) for the ground-truth MPCs, as well as for the MPCs estimated by the five systems. The metrics were plotted versus the T-R distance of the 20 scenarios investigated. The equations for the three metrics are defined below[9]:

$$PL^{VV} = 1/\sum_{n=1}^{N} |a_n^{VV}|^2 \tag{5}$$

[9]Any phase wrapping in (7) was corrected.

$$\sigma_\tau^{VV} = \frac{\sum_{n=1}^{N} |a_n^{VV}|^2 \cdot (\tau_n - \bar{\tau})^2}{\sum_{n=1}^{N} |a_n^{VV}|^2}, \bar{\tau} = \frac{\sum_{n=1}^{N} |a_n^{VV}|^2 \cdot \tau_n}{\sum_{n=1}^{N} |a_n^{VV}|^2} \tag{6}$$

$$\sigma_{\theta^{R,A}}^{VV} = \frac{\sum_{n=1}^{N} |a_n^{VV}|^2 \cdot (\theta_n^{R,A} - \bar{\theta}^{R,A})^2}{\sum_{n=1}^{N} |a_n^{VV}|^2}, \bar{\theta}^{R,A} = \frac{\sum_{n=1}^{N} |a_n^{VV}|^2 \cdot \theta_n^{R,A}}{\sum_{n=1}^{N} |a_n^{VV}|^2} \tag{7}$$

Recall that the scenarios are all in LOS conditions, for which the direct path was 5.4-13.6 dB stronger than the secondary paths; consequently, the pathloss was determined mostly by the direct path, whose high signal-to-interference-plus-noise ratio (SINR) rendered its properties easy to estimate by virtue of its robustness to interference from other multipath and noise. That is why the estimated pathloss

matched up very well with the ground-truth for most systems. The estimation error increased notably for the RMS delay spread. This is because the mean RMS delay, $\bar{\tau}$, in (6) was about equal to the delay of the direct path, τ_1, given the dominance of the direct path. As a result, the contribution of the direct path to σ_τ^{VV} was diminished since $(\tau_1 - \bar{\tau})^2 \approx 0$; in other words, the errors from the secondary paths, which are more difficult to estimate, came to surface. The errors in delay stemmed mostly from the finite bandwidth of the probing signal and whether super-resolution techniques were employed to extract the MPCs. Error in RMS angle spread, rather, was rooted not only in the probing signal and the extraction technique, but also in the finite beamwidth of the antennas and in the array geometry. Given the diversity of the system architectures described in Section II, the large variation in error observed is expected. For the same reasoning as for RMS delay spread, RMS angle spread better reflects error in the secondary paths than pathloss does.

B. One-by-One Comparison of MPCs

Fig. 11(a-e) displays the MPCs estimated by the five channel sounders for the test scenario corresponding to the ground-truth MPCs in Fig. 7(b). Besides the lower dimensional space, it is apparent that the number of estimated MPCs was much less than the number of true MPCs, caused by hardware limitations. In order to cross-validate the estimated MPCs one by one, a mapping between the estimated paths and true paths was first necessary. Our method to obtain the mapping was to solve the assignment problem through the Hungarian method [47], whose objective was to find the one-to-one correspondence that minimized the cumulative absolute error between them. The error was system specific, meaning that it was confined to the property space of the individual system. To mitigate false alarms, the mapping was curtailed by applying thresholds on the error per dimension, which were set nominally as: 4 dB on path gain (a_n^{VV}, a_n^{HH}, a_n^{VH}, and/or a_n^{HV}), 3 ns on delay (τ_n), and 15° on angle ($\theta^{T,A}, \theta^{R,A}, \theta^{T,E}$, and/or $\theta^{R,E}$).

Once the mapping was obtained, the error in all dimensions reported per organization was compiled in Table II (the shaded entries indicate that a particular system does not estimate those properties). The errors were computed by averaging over all mapped MPCs per test scenario and then over all 20 test scenarios. Also compiled in the table were the probabilities of detection / false alarm, i.e. the average percentage of mapped / unmapped MPCs with respect to the total number of ground-truth MPCs. Naturally, the statistics depend on the thresholds set: the more lenient the thresholds, the higher / lower the probabilities of detection / false alarm, but the higher the estimation errors as well. In fact, by varying the thresholds[10], we traced out the full ranges of detection vs. false-alarm probabilities in Fig. 12.

[10]Due to space limitations, the MPC property errors in Table II for varying thresholds were not generated as well.

TABLE II: ONE-TO-ONE COMPARISON OF ESTIMATED MPCs VS. GROUND-TRUTH MPCs

	Prob. detect. (%)	Prob. false alarm (%)	Error $\lvert a^{VV}\rvert^2$ (dB)	Error τ (ns)	Error $\theta^{T,A}$ (deg.)	Error $\theta^{T,E}$ (deg.)	Error $\theta^{R,A}$ (deg.)	Error $\theta^{R,E}$ (deg.)
NIST	7.34	1.71	1.47	0.65			1.79	1.81
UBC	4.39	6.11	1.47	1.44	1.81		1.91	
USC	7.80	0.84	1.53	1.43	1.67		1.71	
NCSU	8.70	1.37	1.65	0.57	5.75	3.42	5.65	3.47
TUI	3.70	3.62	1.47	0.85			2.15	3.5

Because the mapping did not factor in AoD, the results were biased towards relatively lower AoA errors; this affected UBC's system more since the number of estimated MPCs was less than other systems due to filtering in their processing to only the five strongest double-directional scan angles. Otherwise, from our observations, misdetections and estimation errors across all systems were most often attributed to:

- Errors in peak detection due to spatial-temporal sidelobes stemming from limited dynamic range and due to noise stemming from limited link budget;
- Extraction algorithms that do not properly account for the same MPC appearing in multiple antennas, so it is counted multiple times;
- Path splitting [12], in which several closely spaced ghost MPCs were identified by the super-resolution algorithm whereas only a single ground truth path actually existed;
- Superposition of multiple paths beyond the spatial-temporal resolution of the system can distort the properties;
- Complex amplitude was not estimated accurately due to imprecise de-embedding of the antennas and/or poor calibration of the antenna patterns or RF front ends;
- Angle is not estimated properly due to the inherent limitations of the array geometry or coarse scanning resolution.

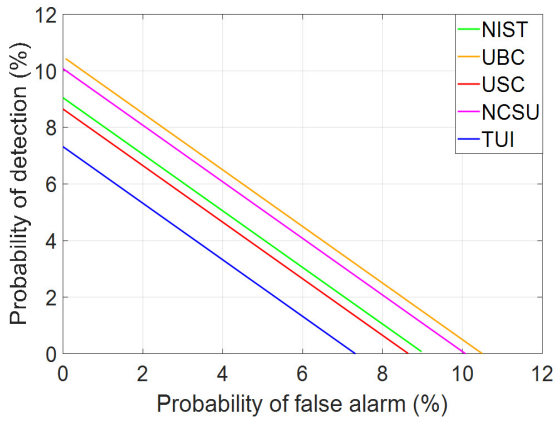

Fig. 12: Probabilities of detection and of false alarm of the estimated MPCs.

V. CONCLUSIONS

To benchmark the performance of radio-frequency channel sounders, we presented a methodology based on a mathematical system model for the sounders whose parameters are

their hardware features measured through in situ calibration procedures to ensure accurate representation. To ensure fairness between the sounders, the system model was applied to the same channel response and results were compared between five worldwide organizations that participated in the cross-validation with their 28-GHz systems. The results of the cross-validation revealed stark differences between the systems for typical large-scale channel metrics: average estimation error for pathloss over 20 test scenarios ranged between 0.7% and 20.6%, for RMS delay spread between 11.3% and 86.1%, and for RMS angle spread between 16.6% and 92.6%. Besides for benchmarking, the methodology proved useful as an analysis tool to highlight the most significant sources of error – e.g. omission of channel paths due to limited spatial-temporal resolution and dynamic range – and were documented accordingly. Finally, shortcomings of the system model – e.g. narrowband assumption for frequency selectivity and planar assumption for wavefronts – were discussed, as were possible extensions in future work to enhance its accuracy.

REFERENCES

[1] 3GPP LTE homepage: https://www.3gpp.org/technologies/keywords-acronyms/98-lte.

[2] IEEE 802.11ay homepage : http://www.ieee802.org/11/Reports/tgay_update.htm.

[3] Correia, Luis M. Wireless flexible personalized communications. John Wiley & Sons, Inc., 2001.

[4] Calcev, George, et al. "A wideband spatial channel model for system-wide simulations." *IEEE Transactions on Vehicular Technology* 56.2 (2007): 389-403.

[5] Almers, Peter, et al. "Survey of channel and radio propagation models for wireless MIMO systems." *EURASIP Journal on Wireless Communications and Networking* 2007.1 (2007): 019070.

[6] Haneda, Katsuyuki. "Channel models and beamforming at millimeter-wave frequency bands." *IEICE Transactions on Communications* 98.5 (2015): 755-772.

[7] Yang Yang. et al. Channel Measurement and Modeling. In: 5G Wireless Systems. Wireless Networks. Springer, Cham, 2018.

[8] Högbom, J. A. "Aperture synthesis with a non-regular distribution of interferometer baselines." *Astronomy and Astrophysics Supplement Series* 15 (1974): 417.

[9] Schmidt, Ralph. "Multiple emitter location and signal parameter estimation." *IEEE transactions on antennas and propagation* 34.3 (1986): 276-280.

[10] Roy, Richard, and Thomas Kailath. "ESPRIT-estimation of signal parameters via rotational invariance techniques." *IEEE Transactions on acoustics, speech, and signal processing* 37.7 (1989): 984-995.

[11] Fessler, Jeffrey A., and Alfred O. Hero. "Space-alternating generalized expectation-maximization algorithm." *IEEE Transactions on signal processing* 42.10 (1994): 2664-2677.

[12] Richter, Andreas. "Estimation of radio channel parameters: Models and algorithms." ISLE, 2005.

[13] 5G mmWave Channel Model Alliance homepage: https://www.nist.gov/ctl/5g-mmwave-channel-model-alliance.

[14] Michelson, David G., et al. "System Distortion Model for the Cross-Validation of Millimeter-Wave Channel Sounders." *2019 13th European Conference on Antennas and Propagation (EuCAP)*. IEEE, 2019.

[15] Papazian, Peter B., et al. "A radio channel sounder for mobile millimeter-wave communications: System implementation and measurement assessment." *IEEE Transactions on Microwave Theory and Techniques* 64.9 (2016): 2924-2932.

[16] Papazian, Peter B., et al. "Calibration of millimeter-wave channel sounders for super-resolution multipath component extraction." *2016 10th European Conference on Antennas and Propagation (EuCAP)*. IEEE, 2016.

[17] Sun, Ruoyu, et al. "Design and calibration of a double-directional 60 GHz channel sounder for multipath component tracking." *2017 11th European Conference on Antennas and Propagation (EUCAP)*. IEEE, 2017.

[18] Gordon, Joshua A., et al. "Millimeter-wave near-field measurements using coordinated robotics." *IEEE Transactions on Antennas and Propagation* 63.12 (2015): 5351-5362.

[19] Liya, Badrun Naher, and David G. Michelson. "Characterization of multipath persistence in device-to-device scenarios at 30 GHz." *2016 IEEE Globecom Workshops (GC Wkshps)*. IEEE, 2016.

[20] Bas, Celalettin Umit, et al. "Real-time millimeter-wave MIMO channel sounder for dynamic directional measurements." *IEEE Transactions on Vehicular Technology* 68.9 (2019): 8775-8789.

[21] Wang, Rui, et al. "Enable super-resolution parameter estimation for mm-wave channel sounding." *arXiv preprint arXiv:1901.07749* (2019).

[22] Khawaja, Wahab, et al. "Coverage Enhancement for mm Wave Communications using Passive Reflectors." *2018 11th Global Symposium on Millimeter Waves (GSMM)*. IEEE, 2018.

[23] Khawaja, Wahab Ali Gulzar, et al. "Effect of passive reflectors for enhancing coverage of 28 GHz mmWave systems in an outdoor setting." *2019 IEEE Radio and Wireless Symposium (RWS)*. IEEE, 2019.

[24] Müller, Robert, et al. "Simultaneous multi-band channel sounding at mm-Wave frequencies." *2016 10th European Conference on Antennas and Propagation (EuCAP)*. IEEE, 2016.

[25] METIS II Project homepage: https://metis-ii.5g-ppp.eu.

[26] MiWEBA Project homepage: http://www.miweba.eu.

[27] mm MAGIC Project homepage: https://5g-mmmagic.eu.

[28] Kunisch, Jürgen, and Jörg Pamp. "An ultra-wideband space-variant multipath indoor radio channel model." *IEEE Conference on Ultra Wideband Systems and Technologies, 2003*. IEEE, 2003.

[29] Maltsev, Alexander, et al. "Quasi-deterministic approach to mmwave channel modeling in a non-stationary environment." *2014 IEEE Globecom Workshops (GC Wkshps)*. IEEE, 2014.

[30] Deng, Sijia, Geoge R. MacCartney, and Theodore S. Rappaport. "Indoor and outdoor 5G diffraction measurements and models at 10, 20, and 26 GHz." *2016 IEEE Global Communications Conference (GLOBECOM)*. IEEE, 2016.

[31] Senic, Jelena, et al. "Analysis of E-band path loss and propagation mechanisms in the indoor environment." *IEEE transactions on antennas and propagation* 65.12 (2017): 6562-6573.

[32] Lai, Chiehping, et al. "Methodology for multipath-component tracking in millimeter-wave channel modeling." *IEEE Transactions on Antennas and Propagation* 67.3 (2018): 1826-1836.

[33] Wen, Zhu, et al. "mmWave channel sounder based on COTS instruments for 5G and indoor channel measurement." *2016 IEEE Wireless Communications and Networking Conference.* IEEE, 2016.

[34] Salous, Sana, et al. "Wideband MIMO channel sounder for radio measurements in the 60 GHz band." *IEEE Transactions on Wireless Communications* 15.4 (2015): 2825-2832.

[35] Mbugua, Allan Wainaina, et al. "Millimeter wave multi-user performance evaluation based on measured channels with virtual antenna array channel sounder." *IEEE Access 6* (2018): 12318-12326.

[36] Weiss, Alec J., et al., "Setup and Control of a mmWave Synthetic Aperture Measurement System with Uncertainties," *Microwave Measurement Conference*, ARFTG, 2020.

[37] Caudill, Derek, et al. "Omnidirectional Channel Sounder With Phased-ArrayAntennas for 5G Mobile Communications." *IEEE Transactions on Microwave Theory and Techniques* 67.7 (2019): 2936-2945.

[38] Maltsev, Alexander, et al. "Experimental investigations of 60 GHz WLAN systems in office environment." *IEEE Journal on Selected Areas in Communications* 27.8 (2009): 1488-1499.

[39] Sawada, Hirokazu, et al. "Impulse response model and parameters for indoor channel modeling at 60GHz." *2010 IEEE 71st Vehicular Technology Conference*. IEEE, 2010.

[40] Hur, Sooyoung, et al. "Synchronous channel sounder using horn antenna and indoor measurements on 28 GHz." *2014 IEEE International Black Sea Conference on Communications and Networking (BlackSeaCom)*. IEEE, 2014.

[41] Akdeniz, Mustafa Riza, et al. "Millimeter wave channel modeling and cellular capacity evaluation." *IEEE journal on selected areas in communications* 32.6 (2014): 1164-1179.

[42] Park, Jae-Joon, et al. "Millimeter-wave channel model parameters for urban microcellular environment based on 28 and 38 GHz measurements." *2016 IEEE 27th Annual International Symposium on Personal, Indoor, and Mobile Radio Communications (PIMRC)*. IEEE, 2016.

[43] MacCartney, George R., and Theodore S. Rappaport. "A flexible millimeter-wave channel sounder with absolute timing." *IEEE Journal on Selected Areas in Communications* 35.6 (2017): 1402-1418..

[44] Salous, Sana, et al. "Millimeter-Wave Propagation: Characterization and modeling toward fifth-generation systems.[Wireless Corner]." *IEEE Antennas and Propagation Magazine* 58.6 (2016): 115-127.

[45] Gentile, Camillo, and Alfred Kik. "A frequency-dependence model for the ultrawideband channel based on propagation events." *IEEE Transactions on Antennas and Propagation* 56.8 (2008): 2775-2780.
[46] Larsson, Erik G., et al. "Massive MIMO for next generation wireless systems." *IEEE communications magazine* 52.2 (2014): 186-195.
[47] Bazaraa, Mokhtar S., John J. Jarvis, and Hanif D. Sherali. *Linear programming and network flows*. John Wiley & Sons, 2011.

Camillo Gentile (M'01) received the Ph.D. degree in electrical engineering from Pennsylvania State University in 2001, with a dissertation on computer vision and artificial intelligence. He joined the National Institute of Standards and Technology in Gaithersburg, Maryland in 2001 and is currently a project leader in the Wireless Networks Division of the Communications Technology Laboratory. He has authored over 80 peer-reviewed journal and conference papers, a book on geolocation techniques, and a book on millimeter-wave channel modeling. His current interests include channel modeling and physical-layer modeling for 5G communications systems.

Andreas F. Molisch received his PhD and habilitation from TU Vienna in 1994 and 1999, respectively. After 10 years in industry he joined the University of Southern California, where he is now the Solomon Golomb – Andrew and Erna Viterbi Chair Professor. His research interest is wireless communications, with emphasis on wireless propagation channels, ultrawideband signaling and localization, multi-antenna systems, novel modulation methods, caching for wireless content distribution, and edge computing. He is the author of four books, 21 book chapters, more than 250 journal papers, 350 conference papers, as well as 80 patents. He is a Fellow of the National Academy of Inventors, IEEE, AAAS, and IET, as well as Member of the Austrian Academy of Sciences and recipient of numerous awards.

Jack Chuang was a graduate research assistant in the Communications and Space Sciences Laboratory (CSSL) at the Pennsylvania State University and obtained his Ph.D. degree in 2008. He then worked at BAE Systems in electronc warfare and at Cisco Systems in spectrum sharing. He is currently with NIST Communication Technology Lab, Gaithersburg, USA, developing 5G mmWave channel sounders.

David G. Michelson received the B.Sc., M.Sc., and Ph.D. in electrical engineering from the University of British Columbia (UBC), Vancouver, BC, Canada. From 1996 to 2001, he served as a member of a joint team from AT&T Wireless Services, Redmond, WA, USA, and AT&T Labs-Research, Red Bank, NJ, USA, where he contributed to the development of propagation and channel models for the next generation and fixed wireless systems. Since 2003, he has led the Radio Science Laboratory in the Department of Electrical & Computer Engineering at UBC. He and a former student received the R.W.P. King Best Paper Award from the IEEE Antennas and Propagation Society in 2011. In Fall 2018, he served as a Guest Researcher with the Wireless Network Division, U.S. National Institute of Standards and Technology. Prof, Michelson currently serves as a member of the Board of Governors and Chair of the Propagation Committee of the IEEE Vehicular Technology Society. He also serves as chair of the Canadian National Committee of the International Union of Radio Science (2018-2021) and Canadian representative to URSI Commission F-Wave Propagation and Remote Sensing (2015-2021). His research interests include propagation and channel modelling, and wireless communications for connected & automated vehicles, advanced marine systems and small satellites.

Anuraag Bodi is working as a contractor in the Wireless Networks Division, National Institute of Standards and Technology, Gaithersburg, Maryland. He received his B.Tech. degree in electronics and communication engineering from Andhra University, Visakhapatnam, India, in 2012 and MS degree in electrical engineering from University of Colorado, Boulder in 2016. He is currently pursuing second MS degree in computer science from Georgia Tech.

Anmol Bhardwaj received the B.A.Sc and M.A.Sc degrees in electrical & computer engineering from the University of British Columbia, Vancouver, BC, Canada. He served as a Guest Researcher with the Communications Technology Laboratory, National Institute of Standards and Technology from October 2017 to December 2018 and then from November 2019 to Present. His research interests include millimeter-wave channel measurements and modeling.

Ozgur Ozdemir received the BS degree in Electrical and Electronics Engineering from Bogazici University, Istanbul, Turkey, in 1999 and the MS and PhD degrees in Electrical Engineering from The University of Texas at Dallas, Richardson, TX, USA, in 2002 and 2007, respectively. From 2007 to 2016 he was an Assistant Professor at Fatih University, Turkey, and worked as a Postdoctoral Scholar at Qatar University for 3.5 years. He joined Department of Electrical and Computer Engineering at North Carolina State University (NCSU) as a visiting research scholar in 2017. He is now working as a Wireless Engineer at NCSU. His research interests include channel sounding for mmWave systems, opportunistic approaches in wireless systems, digital compensation of radio-frequency impairments, and software-defined radios.

Wahab Ali Gulzar Khawaja received his BS and MS degrees both in electrical engineering from University of Engineering and Technology, Lahore, Pakistan in 2008 and 2012, respectively. He received his PhD degree from Electrical and Computer Engineering Department of North Carolina State University on Fulbright scholarship in 2019. He is currently working as an assistant professor at Mirpur University of Science and Technology, Mirpur AJK, Pakistan. His current research areas are UWB channel modeling, mmWave channel modeling using UAVs or static platforms in different environmental conditions, and use of passive and intelligent reflecting surfaces for aiding propagation in NLOS areas.

Ismail Guvenc (senior member, IEEE) has been an Associate Professor at North Carolina State University since August 2016. His recent research interests include 5G wireless networks, UAV communications, and heterogeneous networks. He has published more than 260 conference/journal papers, several standardization contributions, three books, and over 30 U.S. patents. He is a recipient of the 2019 R. Ray Bennett Faculty Fellow Award, 2016 FIU COE Faculty Research Award, 2015 NSF CAREER Award, 2014 Ralph E. Powe Junior Faculty Award, and 2006 USF Outstanding Dissertation Award, and he is a senior member of the National Academy of Inventors.

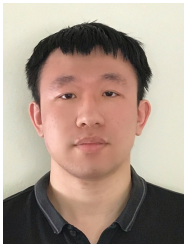

Zihang Cheng is a Ph.D. student in Ming-Hsieh Department of Electrical and Computer Engineering, University of Southern California. He received his B.S. degree in Electrical and Electronics from Tsinghua University, Beijing, China in 2016. His research interests include channel estimation and channel modeling of communication systems. He is also interested in developing estimation algorithms and optimization.

François Rottenberg (S'15–M'18) received the M.Sc. in Electrical Engineering from the Université catholique de Louvain (UCLouvain), Louvain-la-Neuve, in 2014, and the Ph.D. degree jointly from UCLouvain and Université libre de Bruxelles (ULB), Brussels, in 2018. From September 2018 to August 2019, he was a postdoctoral researcher with the University of Southern California (USC), Los Angeles, U.S.A, leading the 5G massive MIMO research efforts. He is now a postdoctoral researcher affiliated with UCLouvain and ULB, funded by the Belgian National Science Foundation (FRS-FNRS). He participated to various national, European and international projects. From 2015, he has been a regular visitor and collaborator of the Centre Tecnològic Telecomunicacions Catalunya (CTTC), Castelldefels, Spain and National Institute of Information and Communications Technology (NICT), Tokyo, Japan. His main research interests are in signal processing for next generations of communication systems, including novel modulation formats, multi-antenna systems and physical-layer security.

Thomas Choi is a Ph.D. student studying electrical and computer engineering at Wireless Devices and Systems (WiDeS) group in University of Southern California (USC). He received a B.S. degree in electrical engineering at USC in 2015 followed by a M.S. degree in aerospace engineering at Georgia Tech in 2017. His current research interests are evaluating and modeling real world wireless channels accurately for modern and future wireless systems through channel sounder developments and channel measurement campaigns.

Robert Müller received the M.S. degree in electronic engineering from the Berlin University of Technology, Berlin, Germany, in 2009 and 2007 the Dipl. Ing. degree in communication technology engineering from BTU Cottbus-Senftenberg. His research includes high-frequency component design, high-frequency front-end design, antenna design, ultrawideband system design, special antenna array design for channel sounding applications and channel sounder design up to THz. His current research interest includes over the over the air test, channel sounding measurement systems (at mmW and THz), and analysis for mmWave communication system in the field of V2V and cellular networks. He also developed investigations in mmWave/THz technologies in the frame of IEEE 802.11/802.15 group. Since 2019, he lead the mmWave and THz Broadband Technology team at Fraunhofer IIS in Ilmenau.

Niu Han received the B.S. degree in electronic information science and technology from the University of ZhengZhou, Zhengzhou, China, in 2011 and the M.S. degree in communications engineering from the University of Duisburg-Essen, Duisburg, Germany, in 2016. Since 2017, he has been with the Electronic Measurement Research Laboratory, Technische Universität Ilmenau, Ilmenau, Germany, where he is currently pursuing the Dr.Ing. degree in electrical engineering. His current research interests include radio channel modeling and ray tracing.

Diego Dupleich received the Engineering degree (Hons.) in electronic engineering from Universidad Tecnológica Nacional, Paraná, Argentina, in 2009, and the M.S. degree (Hons.) in communications and signal processing from Technische Universität Ilmenau, Ilmenau, Germany, in 2013, where he is currently pursuing the Ph.D. degree in electrical engineering. From 2009 to 2010, he was an RF Specialist in satellite communications with Emerging Markets Communications. Since 2013, he has been with the Electronic Measurements and Signal Processing Group, Technische Universität Ilmenau, where he is currently involved in the millimetre-wave field. For his work on channel measurements and modelling, he received the Best Paper Award in Propagation at the 11th European Conference on Antennas and Propagation.